Molecular Therapy
Nucleic Acids
Original Article

Efficient transfected liposomes co-loaded with pNrf2 and pirfenidone improves safe delivery for enhanced pulmonary fibrosis reversion

Xin Chang,[1,2,3,8] Chang Liu,[1] Yu-Mo Han,[1] Qiu-Ling Li,[1] Bin Guo,[1,2,3,8] and Hu-Lin Jiang[4,5,6,7,8]

[1]School of Pharmacy, Jinzhou Medical University, Jinzhou, Liaoning 121001, China; [2]Liaoning Provincial Key Laboratory of Marine Bioactive Substances, Jinzhou Medical University, Jinzhou, Liaoning 121001, China; [3]Technological Innovation Center of Liaoning Pharmaceutical Action and Quality Evaluation, Jinzhou Medical University, Jinzhou, Liaoning 121001, China; [4]State Key Laboratory of Natural Medicines, China Pharmaceutical University, Nanjing, Jiangsu 210009, China; [5]Jiangsu Key Laboratory of Druggability of Biopharmaceuticals, China Pharmaceutical University, Nanjing, Jiangsu 210009, China; [6]Jiangsu Key Laboratory of Drug Discovery for Metabolic Diseases, China Pharmaceutical University, Nanjing, Jiangsu 210009, China; [7]NMPA Key Laboratory for Research and Evaluation of Pharmaceutical Preparations and Excipients, China Pharmaceutical University, Nanjing, Jiangsu 210009, China

Pulmonary fibrosis (PF) is an interstitial lung disease with complex pathological mechanism, and there is currently a lack of therapeutics that can heal it completely. Using gene therapy with drugs provides promising therapeutic strategies for synergistically reversing PF. However, improving the intracellular accumulation and transfection efficiency of therapeutic nucleic acids is still a critical issue that urgently needs to be addressed. Herein, we developed lipid nanoparticles (PEDPs) with high transfection efficiency coloaded with pDNA of nuclear factor erythroid 2-related factor 2 (pNrf2) and pirfenidone (PFD) for PF therapy. PEDPs can penetrate biological barriers, accumulate at the target, and exert therapeutic effects, eventually alleviating the oxidative stress imbalance in type II alveolar epithelial cells (AECs II) and inhibiting myofibroblast overactivation through the synergistic effects of Nrf2 combined with PFD, thus reversing PF. In addition, we systematically engineered various liposomes (LNPs), demonstrated that reducing the polyethylene glycol (PEG) proportion could significantly improve the uptake and transfection efficiency of the LNPs, and proposed a possible mechanism for this influence. This study clearly reveals that controlling the composition ratio of PEG in PEDPs can efficiently deliver therapeutics into AECs II, improve pNrf2 transfection, and synergize with PFD in a prospective strategy to reverse PF.

INTRODUCTION

Pulmonary fibrosis (PF) is a chronic, progressive interstitial lung disease with high morbidity and mortality that is characterized by the abnormal repair of lung tissues and accumulation of extracellular matrix (ECM), which results in complete loss of lung function and even death.[1,2] Recent epidemiological surveys have indicated that there are more than 5 million patients with PF worldwide, and the number of cases is increasing.[3,4] The pathogenesis of PF is complex and poorly understood, but current studies have suggested that it may be closely related to an imbalance in oxidative stress caused by persistent damage to type II alveolar epithelial cells (AECs II) due to decreased nuclear factor erythroid 2-related factor 2 (Nrf2) expression. This leads to the overactivation and dysregulated repair of myofibroblasts in lung tissues, resulting in excessive ECM deposition and eventually the occurrence of PF.[5,6] Pirfenidone (PFD) is a clinically approved drug for the treatment of PF that only slows the progression of PF but can hardly reverse it.[7,8] PFD treatment fails because of its single therapeutic target, as it can only inhibit the abnormal proliferation of myofibroblasts by reducing the levels of overexpressed transforming growth factor β (TGF-β), but cannot effectively repair the abnormally injured AECs II that are the root cause of PF.[9] Therefore, a synergistic combination strategy that inhibits myofibroblast activation and repairs injured AECs II effectively might be a potential therapeutic strategy for the treatment of PF.

Combination therapy with genes with drugs has been widely applied as a promising treatment strategy for acquired and inherited diseases. Compared with treatment with small molecules, gene therapy can regulate the abnormal disordered pathways in cells at the molecular level to compensate for the limitations of the single drug target. However, the therapeutic efficacy of naked nucleic acids (i.e., pDNA) is limited by their poor stability and low delivery and intracellular transfection efficiency.[10] In combination therapy, there are several factors that reduce synergistic therapeutic effects, such as poor penetration of pDNA and drugs into cell membranes and their susceptibility to degradation by circulating nucleases.[11] Nonviral carriers such as cationic liposomes (LNPs) provide a reliable and efficacious method

Received 19 December 2022; accepted 6 April 2023;
https://doi.org/10.1016/j.omtn.2023.04.006.

[8]These authors contributed equally

Correspondence: Xin Chang, School of Pharmacy, Jinzhou Medical University, Jinzhou, Liaoning 121001, China.
E-mail: cx0924@jzmu.edu.cn
Correspondence: Bin Guo, School of Pharmacy, Jinzhou Medical University, Jinzhou, Liaoning 121001, China.
E-mail: jyguobin@126.com
Correspondence: Hu-Lin Jiang, State Key Laboratory of Natural Medicines, China Pharmaceutical University, Nanjing, Jiangsu 210009, China.
E-mail: jianghulin3@163.com

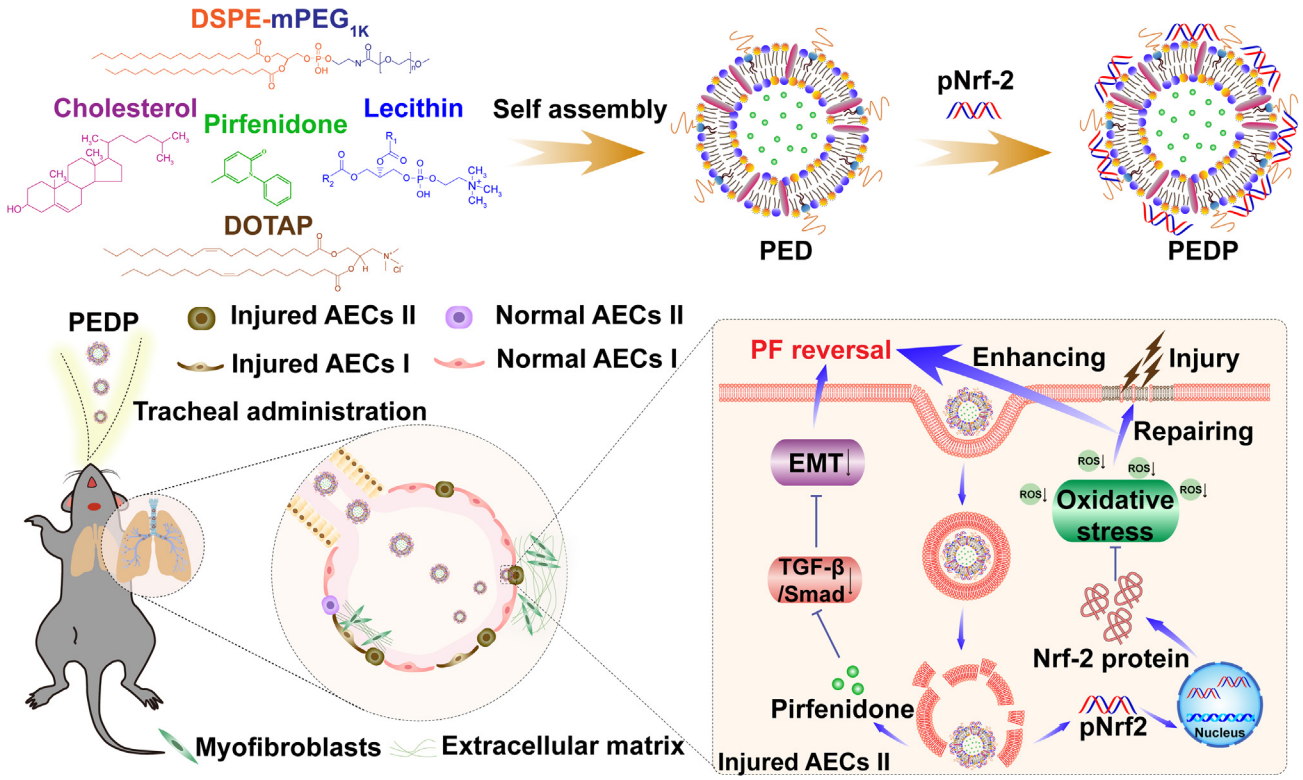

Figure 1. Tracheal administration of PEDP co-loaded with pNrf2 and PFD for PF therapy

PFD and pNrf2 are released in lysosomes of AECs II by pH sensitivity, pNrf2 can enhance the effect of PFD inhibition overactivation of myofibroblasts by alleviating AECs II oxidative stress, and which reverse PF through a gene synergistic drug strategy.

for compound delivery that exhibits the advantages of superior biocompatibility and high loading capacity of therapeutics (i.e., pDNA and drugs). To date, there are several clinical studies using intranasally administered LNPs loaded with pDNA for disease therapy, are where the LNPs/pDNA formulations are guided into cells to regulate cellular homeostasis (ClinicalTrials.gov identifiers NCT00004806 and NCT00004471). However, the intracellular accumulation of LNPs after clinical administration is low, causing low transfection efficiency, which is a major obstacle in the application of LNPs for the treatment of diseases.[12,13] Therefore, there is an urgent need to develop LNPs with high transfection efficiency for enhancing or even reversing PF.

Polyethylene glycol (PEG) is commonly added to LNPs to achieve a long circulation time, reducing their recognition by the mononuclear phagocyte system (MPS) by forming an external hydration layer on the LNPs, which prevents particle aggregation and improves circulation time, leading to enhanced pDNA transfection efficiency *in vivo*.[14–16] However, the PEG component on the surface could expand the hydration volume of the LNPs, which might shield the surface charge density of cationic LNPs and impede cellular internalization of LNP complexes.[17–19] Although LNPs are widely used for gene transfection, it is currently difficult to predict whether the designed LNPs will have satisfactory transfection efficiency and excellent biosafety, which are features that are closely related to the formulation and electrical properties of the LNPs. Therefore, it is of great significance to design and construct LNPs with high transfection efficiency according to the appropriate mechanisms for PF therapy.

In this work, we validated the hypothesis that PEG alters gene transfection efficiency, providing a new approach for the design of predictable and efficient transfection by LNPs. PF reversal was achieved by adding a certain mass ratio of 1,2-distearoyl-sn-glycero-3-phosphoethanolamine-N-[methoxy(polyethylene glycol)$_{1K}$] (DSPE-PEG$_{1K}$) to LNPs for the efficient delivery of therapeutics to treat PF (Figure 1). In general, the oxidative stress injury in AECs II promotes TGF-β release caused by decreased Nrf2 expression, resulting in the excessive activation of myofibroblasts, abundant accumulation of ECM in lung tissues and eventually, the progression of PF.[20,21] In the clinic, PFD can only treat PF by inhibiting the abnormal proliferation of myofibroblasts, but it cannot regulate injured AECs II.[22] However, the imbalance in intracellular oxidative stress in AECs II plays a crucial role in accelerating myofibroblast activation and PF.[23] Effectively regulating the normalization of injured AECs II is a pivotal strategy that could enhance the efficacy of PFD in the treatment of PF. To verify the above hypothesis, in this study, we developed LNPs (PEDPs) coloaded with PFD and pNrf2 to reverse PF through a synergistic molecular and genetic strategy to maximize the therapeutic

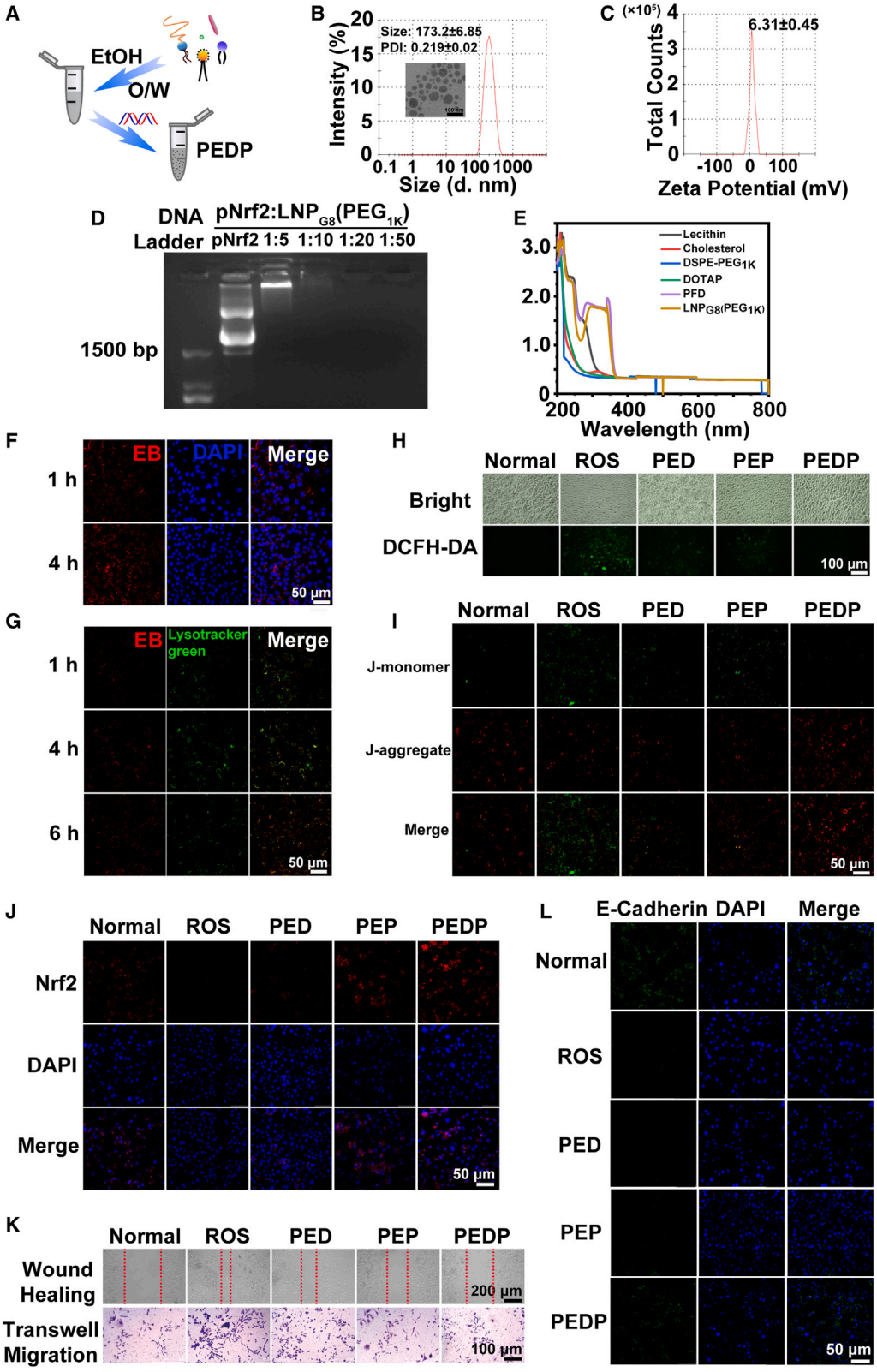

(legend on next page)

effect. Indeed, pNrf2 rapidly entered AECs II with the help of LNPs, alleviated the oxidative stress imbalance and repaired the abnormal damage to AECs II by increasing the expression of the Nrf2 protein. Moreover, PEDPs synergistically inhibited the excessive accumulation of ECM by inhibiting the overactivation of myofibroblasts, thereby blocking the progression of PF and finally reversing this disease. In addition, on the basis of traditional transfection materials that use amphiphilic phospholipids, cationic lipids, PEG, and cholesterol, we built LNPs with various molecular compositions by adding PEG of different molecular weights. We found that reducing both the molecular weight of PEG and its proportion in the LNPs significantly improved the pDNA transfection efficiency of the LNPs, which is a significant finding in the development of LNPs with high transfection efficiency.

RESULTS

Construction and antifibrotic efficacy of $LNP_{G8}(PEG_{1K})$ complexes *in vitro*

$LNP_{G8}(PEG_{1K})$ loaded with PFD was first constructed by the emulsification-solvent evaporation method[24] in which pNrf2 was packaged through positive and negative charge binding forces to generate $LNP_{G8}(PEG_{1K})$/pNrf2@PFD (PEDPs) (Figure 2A). The vesicle size of $LNP_{G8}(PEG_{1K})$ was 173.2 ± 6.85, the PDI was 0.219 ± 0.02, and the morphology of PEDP was homogeneous and sphere-like as characterized by transmission electron microscopy (TEM) (Figure 2B). The zeta potential of PEDP was 6.31 ± 0.45 mV, which is profitable for pDNA loading, delivery efficiency, and excellent gene transfection (Figure 2C). To verify the ability of $LNP_{G8}(PEG_{1K})$ to load pNrf2, we carried out gel electrophoresis assay to determine the optimal ratio of pNrf2 to $LNP_{G8}(PEG_{1K})$. The results showed that the loading rate of pNrf2 was 100% when pNrf2:$LNP_{G8}(PEG_{1K})$ = 1:20 (wt/wt) (Figure 2D). As shown in Figure 2E, PFD was successfully loaded within $LNP_{G8}(PEG_{1K})$ with a loading efficiency of 1.2%. Given the capacity of the $LNP_{G8}(PEG_{1K})$ with efficient pDNA transfection, we applied our findings to evaluate the antifibrosis efficacy of $LNP_{G8}(PEG_{1K})$/pNrf2. We first assessed the cellular uptake of ethidium bromide (EB)-stained $LNP_{G8}(PEG_{1K})$/pNrf2 at different times (1 and 4 h) and found that uptake occurred in a time-dependent manner (Figure 2F). To examine the intracellular fate of $LNP_{G8}(PEG_{1K})$/pNrf2, the colocalization of EB-stained $LNP_{G8}(PEG_{1K})$/pNrf2 with lysosomes was evaluated by confocal laser scanning microscopy (CLSM). As shown in Figure 2G, EB-stained $LNP_{G8}(PEG_{1K})$/pNrf2 (red) were located on the cell membrane at 1 h, then entered the cells and overlapped with the lysosomes (green) to appear yellow at 4 h. Next, the red LNPs separated from the green lysosomes, indicating that EB-stained $LNP_{G8}(PEG_{1K})$/pNrf2 had achieved lysosomal escape at 6 h. PF is caused by oxidative stress in AECs II, and Nrf2 is the central regulator of the maintenance of intracellular redox homeostasis. Herein, we developed LNPs with high transfection efficiency to deliver pNrf2 and PFD into AECs II and alleviate cytosolic oxidative stress. The experimental groups consisted of the normal, reactive oxygen species (ROS), pNrf2-loaded $LNP_{G8}(PEG_{1K})$ (PEP), PFD-loaded $LNP_{G8}(PEG_{1K})$ (PED), and pNrf2 and PFD coloaded $LNP_{G8}(PEG_{1K})$ (PEDP) groups. First, we evaluated the abilities of the various treatments (PEP, PED, and PEDP) to regulate oxidative stress in AECs II by detecting the intracellular ROS content. The results showed that there was the lowest ROS content in the PEDP group, which indicated that PEDP had a better capacity to protect AECs II than the other treatments because of the synergistic effect of pNrf2 with PFD (Figure 2H). In addition, we examined the mitochondrial membrane potential (MMP) to evaluate mitochondrial function in AECs II after treatment. The results showed that the MMP in the PEDP group was similar to that in the normal group, indicating that PEDP had the best therapeutic efficacy to repair oxidative stress in AECs II among the other treatment groups (Figure 2I). To confirm the transfection efficiency by the LNPs and the antioxidative efficacy of various treatments, we assessed Nrf2 expression by immunofluorescence staining. Nrf2 expression was highest in the PEDP group and similar to that in the normal group, which is useful for alleviating oxidative stress (Figure 2J). Then, we evaluated the abilities of various treatments to modulate cellular oxidative stress via Transwell migration and wound healing assays. Excessive cellular oxidative stress could lead to epithelial mesenchymal transition (EMT), which would enhance the migration ability of AECs II and promote PF progression. The results showed that the PEDP treatment effectively inhibited EMT by repairing injured AECs II to appear normal compared with the other treatments, which is the first step for PF reversion (Figure 2K). In addition, we also examined the abilities of the different treatments to inhibit EMT by immunofluorescence staining. The loss of epithelial cadherin (E-cadherin) expression is a hallmark of EMT in AECs II. As shown in Figure 2L, the expression of E-cadherin was significantly decreased in the PEDP group compared with the PED and PEP groups, indicating that efficient expression of the Nrf2 protein could synergistically with PFD inhibit oxidative stress and EMT in AECs II for PF therapy.

Biodistribution of the $LNP_{G8}(PEG_{1K})$ complexes *in vivo*

To verify the therapeutic efficacy of $LNP_{G8}(PEG_{1K})$/pNrf2 to reverse PF, we first evaluated the biodistribution of 1,1′-dioctadecyl-3,3,3,3′-tetramethylindocarbocyanine iodide (DiI)-labeled $LNP_{G8}(PEG_{1K})$/pNrf2

Figure 2. Construction and antifibrotic efficacy of $LNP_{G8}(PEG_{1K})$ complexes *in vitro*

(A) The construction schematic of $LNP_{G8}(PEG_{1K})$. (B) The vesicle sizes and the morphology of $LNP_{G8}(PEG_{1K})$ were detected using the Zetasizer Nano ZS and TEM, respectively. (C) The zeta potential of Zetasizer Nano ZS was evaluated using the Zetasizer Nano ZS. (D) The loading efficiency of LNP to pNrf2 was evaluated using gel electrophoresis assay. (E) The absorption wavelength spectrum of PFD and excipients was detected by ultraviolet-visible spectrophotometer. (F) The uptake efficiency of EB-stained $LNP_{G8}(PEG_{1K})$/pDNA was demonstrated using CLSM at 1 and 4 h. (G) The evaluation of lysosomal escape ability of EB-stained $LNP_{G8}(PEG_{1K})$/pDNA at different time points. (H) Intracellular ROS content of A549 after treatment with PED, PEP, and PEDP. (I) MMP changes were detected using inverted fluorescence microscopy in PED, PEP, and PEDP groups. (J) Nrf2 expression was evaluated using CLSM. (K) Cell migration ability was assessed using wound healing and Transwell migration assay. (L) The expression of E-cadherin was evaluated using CLSM.

using IVIS imaging to evaluate lung-targeted delivery. As shown in Figure 3A, DiI-labeled $LNP_{G8}(PEG_{1K})$/pNrf2 displayed abundant accumulation in fibrotic lungs compared with free DiI at all time points examined, which is valuable for PF treatment. The accumulation of DiI-labeled $LNP_{G8}(PEG_{1K})$/pNrf2 in lung tissues was the highest at 8 h. In addition, we examined the ability of DiI-labeled $LNP_{G8}(PEG_{1K})$/pNrf2 to target AECs II by immunofluorescence staining. At 1 h and 8 h, the green fluorescence from surfactant protein C (SPC)-labeled AECs II overlapped with the red fluorescence from the LNPs, which demonstrated that DiI-labeled $LNP_{G8}(PEG_{1K})$/pNrf2 had a certain affinity for AECs II. The red fluorescence then separated from the green fluorescence at 24 h, indicating that the LNPs were successfully internalized by AECs II and for proper functioning (Figure 3B). In addition, we examined the transfection ability of $LNP_{G8}(PEG_{1K})$/pNrf2-GFP in fibrotic lung tissues *in vivo*, which is a key factor in evaluating therapeutic efficacy. $LNP_{G8}(PEG_{1K})$/pNrf2-GFP displayed distinct green fluorescence, demonstrating that $LNP_{G8}(PEG_{1K})$ had an efficient transfection ability in the PF mouse model, which could promote the high expression of pNrf2 in pulmonary fibrotic tissues, thus improving the antifibrosis efficacy by alleviating oxidative stress in AECs II (Figure 3C). In addition, we detected the expression level of $LNP_{G8}(PEG_{1K})$/pNrf2-GFP by immunofluorescence staining to evaluate the transfection efficiency, and the data were consistent with the results of IVIS imaging (Figure 3D).

Antifibrotic effect of $LNP_{G8}(PEG_{1K})$/pNrf2 *in vivo*

Given the transfection efficiency and anti-PF potential of $LNP_{G8}(PEG_{1K})$/pNrf2 *in vitro*, we assessed its antifibrosis efficacy in PF mice (Figure 4A). First, we evaluated inflammatory cell proliferation and collagen accumulation in the lung tissues from mice in different treatment groups using H&E staining and Masson trichrome staining, respectively. The results of H&E staining showed that the morphology of the lung tissues from the PEDP group was similar to the normal morphology, but the lung tissues from the bleomycin sulfate (BLM) group and PED and PEP groups were all destroyed to varying degrees. Among them, the BLM group displayed the most inflammatory cell proliferation and the lung structure was the most seriously damaged, followed by the PED and PEP groups (Figure 4B). Masson trichrome staining showed that the tissue from the PEDP group had the least collagen accumulation and the best anti-PF treatment effect, followed by the tissue from other treatments, and PED treatment was the worst among all treatment groups, which indicated that inhibiting myofibroblast activation alone did not block PF progression (Figure 4C). In addition, we examined the proliferation of inflammatory cells in the blood of the mice, including white blood cells, lymphocytes, monocytes, and neutrophils. The results demonstrated that PEDP inhibited the inflammatory response at the beginning of PF compared with other treatment groups, showing that this therapy is conducive to the achieving effective PF treatment (Figure 4D). Studies have confirmed that oxidative stress imbalances in lung tissues play a crucial role in the early stages of PF progression. Therefore, we detected the biochemical indicators associated with oxidative stress, including superoxide dismutase (SOD), glutathione (GSH), and malondialdehyde (MDA). The results indicated that PEDP effectively alleviated abnormal oxidative stress in PF and was more effective than the other treatments (Figures 4E–4G). Furthermore, Nrf2 is the transcription factor that regulates antioxidant stress and plays an important role in inducing the antioxidant response during early PF progression. To explore the antifibrotic mechanism of $LNP_{G8}(PEG_{1K})$/pNrf2, we assessed the expression of the Nrf2 protein using immunofluorescence staining and ELISA. The expression level of the Nrf2 protein was the highest in the PEDP group, which is beneficial for PF therapy (Figures 4H and 4I). These results demonstrated that PEDP could effectively regulate the balance of oxidative stress in fibrotic lung tissues. We then assessed the expression of E-cadherin, an important signaling molecule that regulates the adhesion between AECs II and maintains cell structure and integrity. E-cadherin expression in the PEDP group was similar to that in the normal group and significantly upregulated compared with that in the other treatment groups (PED and PEP) (Figure 4J), which indicated that PEDP could effectively repair the damage to AECs II and promote normalization, which are good for PF therapy. Moreover, to further validate the synergistic antifibrotic effect of gene/drug combination therapy, we detected the expression of α-smooth muscle actin (α-SMA) and the accumulation of collagen I. As shown in Figures 4K and 4L, the immunofluorescence staining and ELISA results showed that PEDP effectively downregulated α-SMA expression by inhibiting myofibroblast activation and proliferation, thus reducing collagen I accumulation in lung tissues. In addition, collagen I accumulation was also detected using immunofluorescence staining. The results showed that PEDP administration resulted in minimal collagen I accumulation compared with collagen I accumulation in the other treatment groups, demonstrating that PEDP had the best therapeutic effect among all treatment groups (Figure 4M).

Evaluation of the biosafety of the LNP preparations

To evaluate the biosafety of the LNP preparations, we examined a variety of biochemical indicators to explore their toxicity to other organs. As shown in Figures 5A–5C, the alanine aminotransferase (ALT), aspartate aminotransferase (AST), and blood urea nitrogen (BUN) levels were the lowest compared with other treatments, and the levels in all treatment groups were in the normal ranges. In addition, we assessed damage to different organs by H&E staining. The results showed that the morphology of the liver, heart, spleen, and kidneys did not change significantly after administration of PED, PEP, and PEDP compared with the normal group (Figure 5D). In addition, the weights of the mice were monitored daily after administrating the various treatments (Figure S1). All of these results indicated that PED, PEP, and PEDP had good biosafety and were suitable for antifibrosis therapy.

Discovery, performance, and development of the LNP preparations

LNPs used to deliver pDNA, small interfering RNA (siRNA), and mRNA typically contain four components, including amphiphilic phospholipids, cholesterol, cationic phospholipids, and lipid PEG,

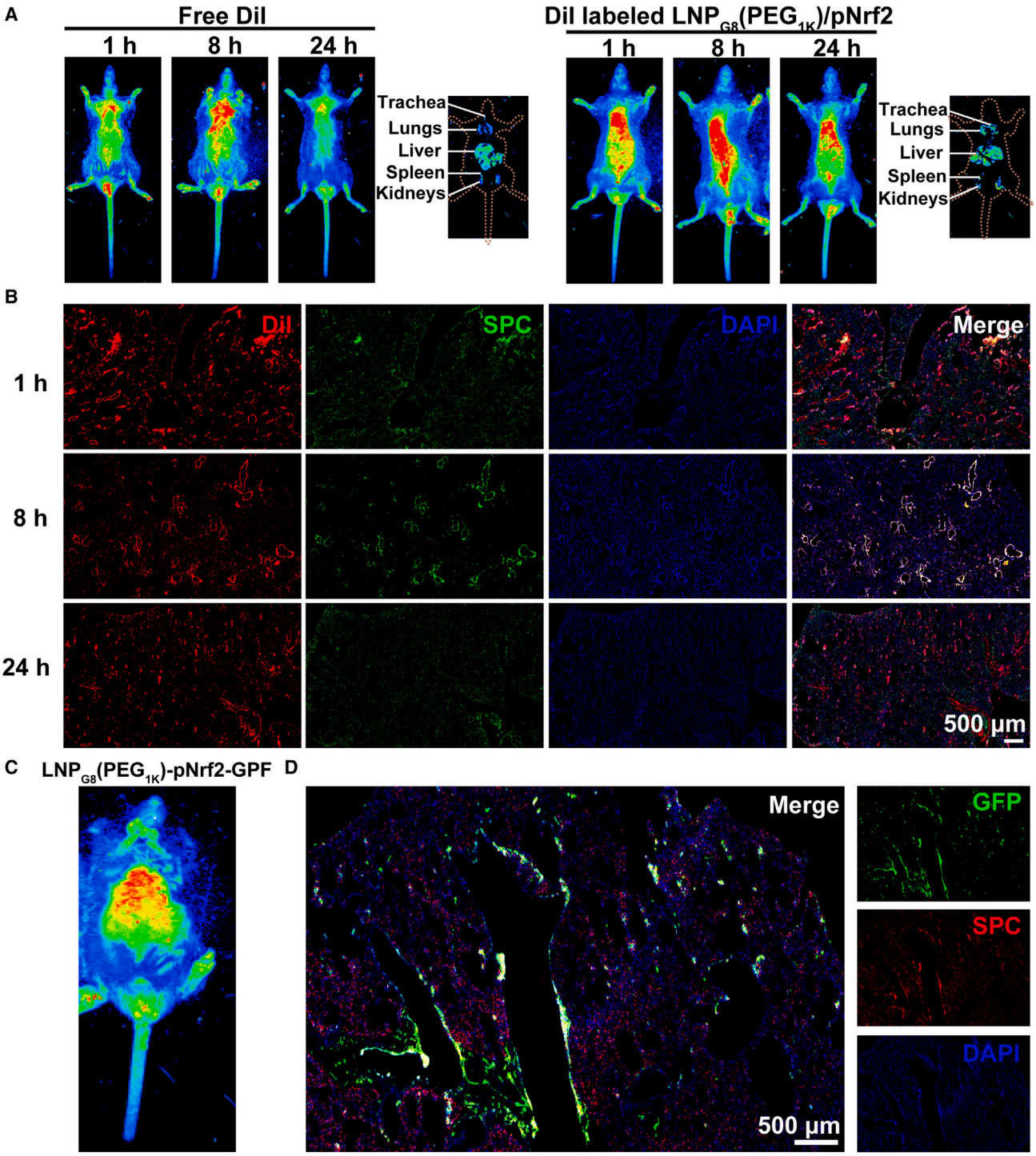

Figure 3. Biodistribution of the LNP$_{G8}$(PEG$_{1K}$)/pDNA *in vivo*

(A) The biodistribution of free DiI and DiI-labeled LNP$_{G8}$(PEG$_{1K}$)/pNrf2 was evaluated using the IVIS imaging system at 1, 8, and 24 h. (B) The accumulation of DiI-labeled LNP$_{G8}$(PEG$_{1K}$)/pNrf2 in AECs II by immunofluorescence staining at different times. (C) The expression of LNP$_{G8}$(PEG$_{1K}$)/pNrf2-GFP was assessed using IVIS Spectrum. (D) The LNP$_{G8}$(PEG$_{1K}$)/pNrf2-GFP expression was detected using immunofluorescence staining.

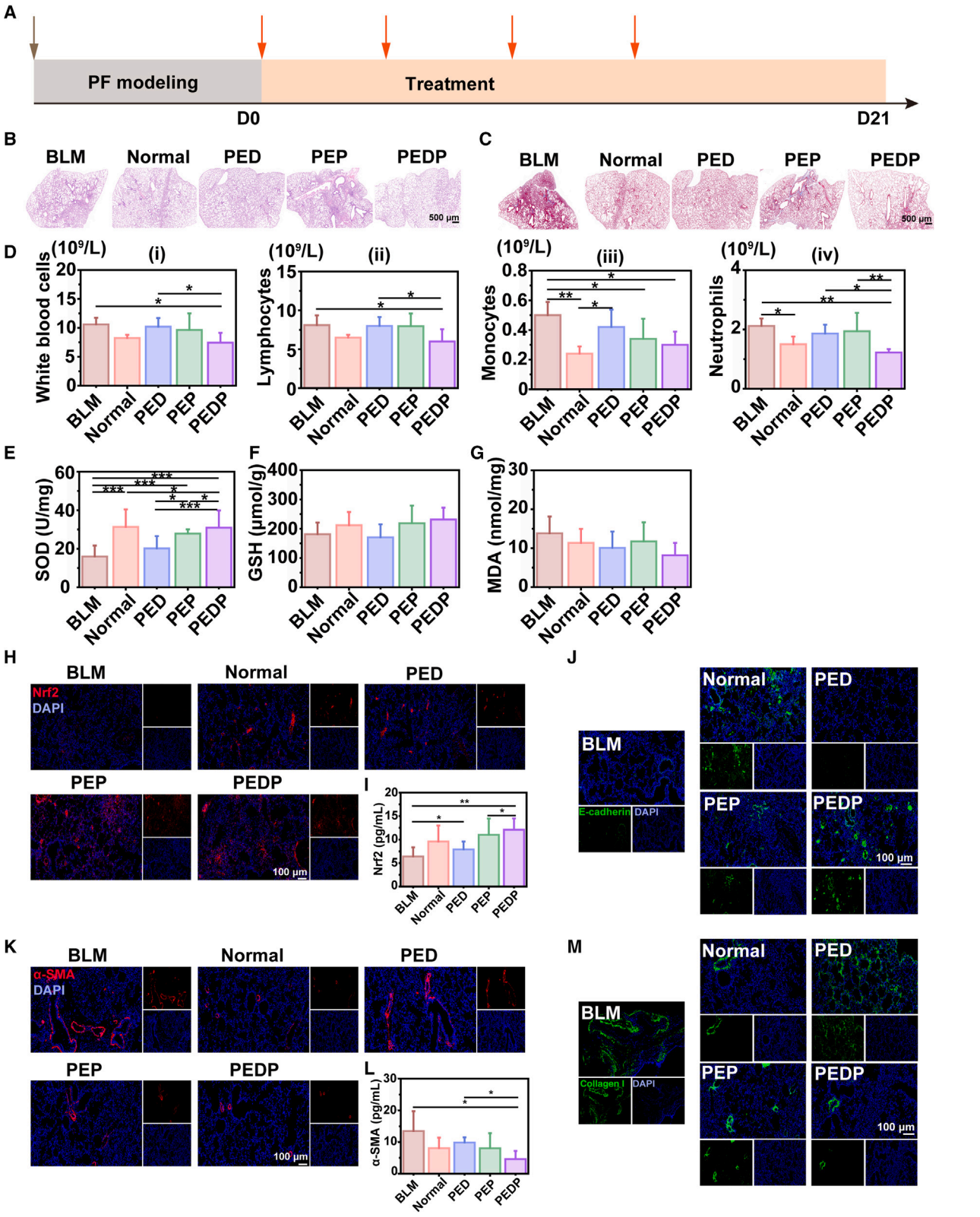

(legend on next page)

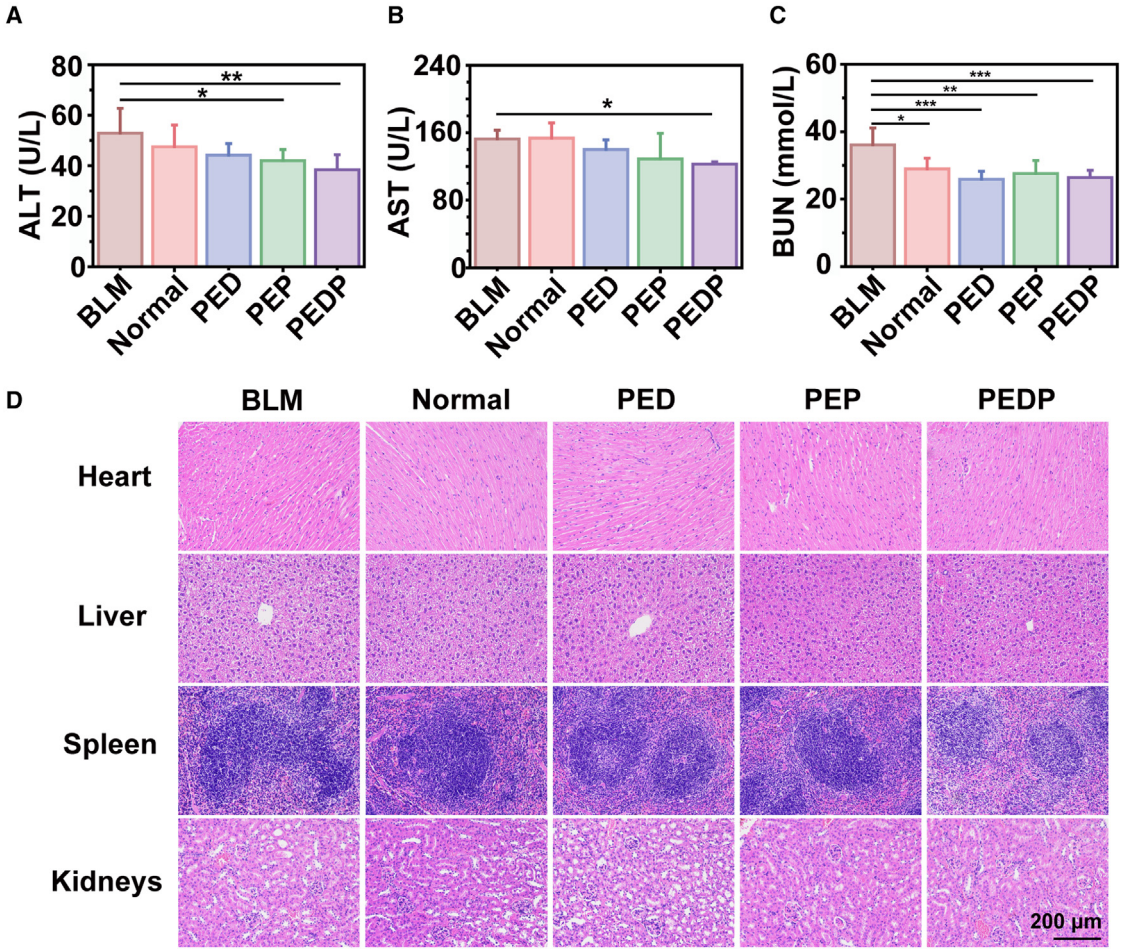

Figure 5. Evaluation of the biosafety of the LNP preparations

(A–C) The content of ALT, AST, and BUN was detected after treating with PED, PEP, and PEDP. (D) The morphologies of liver, heart, spleen, and kidneys in BLM, normal, PED, PEP, and PEDP groups. *p < 0.05, **p < 0.01, and ***p < 0.001.

and differences in their composition or proportions directly affect gene transfection efficiency. To validate the hypothesis that the intrinsic hydration layer formed on the LNPs by PEG would shield their charge and affect gene transfection, we prepared LNPs with different ratios of PEG to find LNPs with remarkable transfection efficiency in AECs II. First, we prepared various LNPs ($LNP_{[G1-G9]}$), which consisted of four parts: part I was lecithin; part II was cholesterol (part I/part II = 2:1, wt/wt); part III was 1,2-distearoyl-sn-glycero-3-phosphoethanolamine-N-[methoxy (polyethylene glycol)] ($DSPE\text{-}PEG_{2K}$) in LNP preparations, the ratios of part I to part III were 1:1 in $LNP_{(G1,\ G4,\ and\ G7)}$, 2:1 in $LNP_{(G2,\ G5,\ and\ G8)}$, 1:2 in $LNP_{(G3,\ G6,\ and\ G9)}$, (wt/wt), part IV was 2,3-dioleoyl-propyl-trimethylammonium chloride (DOTAP), DOTAP/part (I + II + III) = 1:2 in $LNPs_{(G1,\ G2,\ and\ G3)}$, 1:1 in $LNPs_{(G4,\ G5,\ and\ G6)}$, 2:1 in $LNPs_{(G7,\ G8,\ and\ G9)}$ (wt/wt) (Figure 6A). The vesicle sizes and zeta potentials were measured with a Zetasizer Nano ZS (Malvern, UK) (Figure 6B). The results showed that increasing the $DSPE\text{-}PEG_{2K}$ content resulted in LNPs with small vesicle sizes, and the zeta potentials were similar between the different preparations. We then used $LNP_{(G1-G9)}$ to load pDNA in different

Figure 4. Antifibrotic effect of $LNP_{G8}(PEG_{1K})$/pNrf2 *in vivo*

(A) Schematic of animal experiment modeling and drug administration. (B) The pathological feature was evaluated using H&E staining. (C) The accumulation of collagen I was detected using Masson trichrome staining. (D) The proliferation of inflammatory cells (white blood cells, lymphocytes, monocytes, and neutrophils) after treatment with various groups. (E–G) The content of SOD, GSH, and MDA was detected using ELISA. (H) The expression of Nrf2 protein was evaluated using immunofluorescence staining. (I) Nrf2 expression was detected by ELISA. (J) E-cadherin expression was demonstrated using immunofluorescence staining after treating with different groups. (K and L) α-SMA expression was evaluated using immunofluorescence staining and ELISA. (M) The expression of collagen I was evaluated using immunofluorescence staining. *p < 0.05, **p < 0.01, and ***p < 0.001.

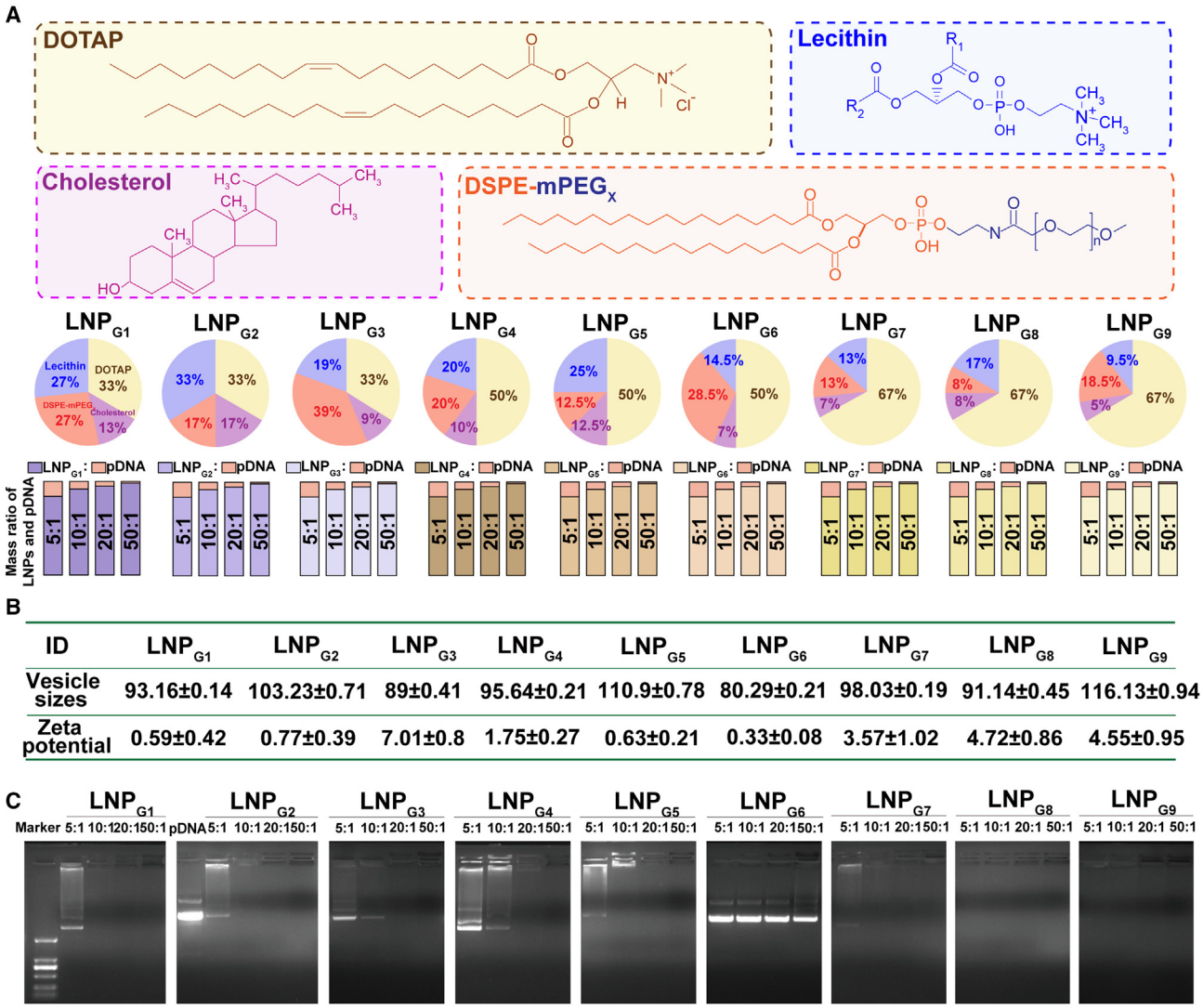

ID	LNP_{G1}	LNP_{G2}	LNP_{G3}	LNP_{G4}	LNP_{G5}	LNP_{G6}	LNP_{G7}	LNP_{G8}	LNP_{G9}
Vesicle sizes	93.16±0.14	103.23±0.71	89±0.41	95.64±0.21	110.9±0.78	80.29±0.21	98.03±0.19	91.14±0.45	116.13±0.94
Zeta potential	0.59±0.42	0.77±0.39	7.01±0.8	1.75±0.27	0.63±0.21	0.33±0.08	3.57±1.02	4.72±0.86	4.55±0.95

Figure 6. Discovery, performance, and development of the LNP preparations

(A) The schematic of LNP preparations. (B) The vesicle sizes and zeta potential were measured using the Zetasizer Nano ZS. (C) The encapsulation capacity was assessed using gel electrophoresis assay.

proportions to investigate gene transfection efficiency (DOTAP/pECFP = 5:1, 10:1, 20:1, or 50:1). Gel electrophoresis assay showed that increasing the content of DOTAP was beneficial to improve the pDNA condensation ability in $LNP_{(G1–G9)}$ (Figure 6C).

Transfection efficiency of the LNP preparations

Increasing cationic percentage could effectively promote intracellular gene transfection, but an excess of DOTAP is cytotoxic. Herein, we first examined the optimal concentration of DOTAP for transfection with a 3-(4,5-dimethyl-2-thiazolyl)-2,5-diphenyl-2-H-tetrazolium bromide (MTT) assay (Figure 7A). The results showed that the viability of the cells treated with the LNP/pECFP complexes (DOTAP/pECFP = 50:1) was less than 50%. Therefore, we chose a DOTAP/pECFP ratio of 20:1 for the following experiments. We then evaluated the efficiency of DiI-labeled LNP/pECFP complex uptake by AECs II by CLSM to explore the influencing factors of the different preparations (Figure 7B). The results showed that the DiI-labeled LNP_{G2}/pECFP, LNP_{G5}/pECFP, and LNP_{G8}/pECFP complexes had higher uptake efficiency. These three groups had the smallest amounts of PEG among the selected groups, which indicated that increasing the proportion of PEG would decrease the efficiency by which the preparations are taken up by cells if the proportion of DOTAP remained the same. In addition, the DiI-labeled LNP_{G2}/pECFP, LNP_{G5}/pECFP, and LNP_{G8}/pECFP complexes had better lysosomal escape abilities than the other groups, which increased the expression level of the target pDNA in AECs II (Figure 7C).

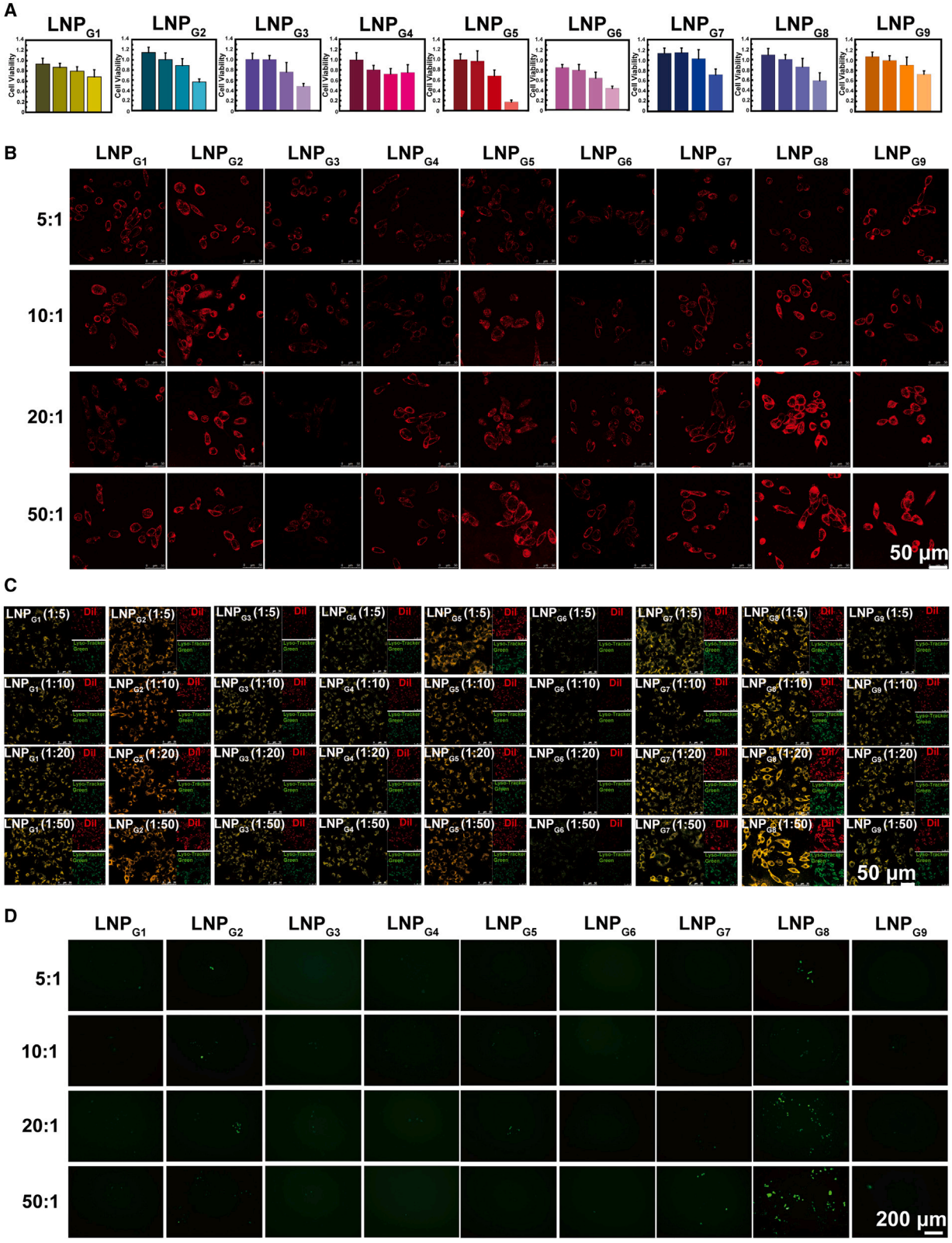

(legend on next page)

We then evaluated the transfection efficiency provided by LNP complexes with various ratios ($LNP_{[G1–G9]}$/pECFP complexes) incubated with A549 cells at a dose of 2 μg/well pECFP. The results demonstrated that the LNP_{G2}/pECFP, LNP_{G5}/pECFP, and LNP_{G8}/pECFP complexes had better transfection efficiency than the other preparations with the same percentages of PEG. In addition, among the three groups with the same percentage of DOTAP but different percentages of PEG (LNP_{G7}/pECFP, LNP_{G8}/pECFP, and LNP_{G9}/pECFP), the results showed that LNP_{G8}/pECFP had the best transfection efficiency, indicating that PEG was the most important factor affecting transfection efficiency in addition to DOTAP (Figure 7D). Therefore, the ratio of PEG components in LNP preparations may be a pivotal factor affecting their cellular uptake efficiency and transfection ability.

Mechanisms affecting transfection efficiency

Inspired by these findings, we hypothesized that the presence or absence of PEG in LNPs would have a significant effect on gene transfection efficiency. On this basis, we examined the influence of the hydration layer of the LNPs on the transfection efficiency by modifying the PEG percentage in the LNP_{G8} formulation, including $LNP_{G8}(PEG_{20\%})$, $LNP_{G8}(PEG_{10\%})$, and $LNP_{G8}(PEG_{0\%})$. The vesicle sizes of these three formulations were 123.4 ± 2.08 (PDI: 0.346 ± 0.001), 119.7 ± 2.04 (0.226 ± 0.007), and 164.2 ± 4.03 (0.362 ± 0.036), respectively (Figure 8A). To prove the importance of the PEG percentage in the LNP preparation on gene transfection ability, we examined the uptake efficiency and transfection ability of $LNP_{G8}(PEG_{20\%})$/pNrf2-GFP, $LNP_{G8}(PEG_{10\%})$/pNrf2-GFP, and $LNP_{G8}(PEG_{0\%})$/pNrf2-GFP. The results showed that $LNP_{G8}(PEG_{0\%})$ and $LNP_{G8}(PEG_{10\%})$ had better uptake efficiency and transfection ability in A549 cells (Figure 8B). Then, we also explored the transfection efficiency of $LNP_{G8}(PEG_{0\%})$/pNrf2-GFP in SMC 7721 cells (Figure S2), and the results were similar to those in A549 cells. In addition, $LNP_{G8}(PEG_{0\%})$/pNrf2-GFP and $LNP_{G8}(PEG_{10\%})$/pNrf2-GFP showed better transfection efficiency than Lipofectamine 3000 (lipo 3000) (Figure S3). We next detected the vesicle sizes of homogeneous and nonhomogeneous LNPs and verified the effect of this parameter on gene transfection efficiency. The results demonstrated that vesicle size had little influence on pNrf2-GFP transfection efficiency (Table S1; Figure S4). The cellular uptake efficiency of LNPs was also a significant factor affecting pNrf2-GFP transfection. Hence, we explored the uptake mechanism of $LNP_{G8}(PEG_{20\%})$, $LNP_{G8}(PEG_{10\%})$, and $LNP_{G8}(PEG_{0\%})$ to investigate whether LNP uptake affected gene transfection. Additionally, the inhibition of uptake was quantified. The results showed that the fluorescence intensity in the $LNP_{G8}(PEG_{0\%})$/pNrf2-GFP group was higher, which indicated that this material would have more opportunities to be taken up by cells (Figure 8C). Uptake mechanism studies revealed that the LNPs entered cells mainly by clathrin-mediated endocytosis as determined by using chlorpromazine, a clathrin-mediated endocytosis inhibitor, which is consistent with existing reports that positively charged particles enter cells mainly through this mechanism.[25] Other inhibitors, including chloroquine (a lipid raft-mediated endocytosis inhibitor), 5-(N-ethyl-N-isopropyl) amiloride (EIPA) (a macropinocytosis inhibitor), and β-cyclodextrin (a caveolae-mediated endocytosis inhibitor), had no significant effect on the uptake of LNPs. Therefore, we reasonably speculated on the basis of the available evidence that the positive charge of the LNPs was the main factor affecting their uptake by cells. Adjusting the percentage of PEG would change the size of the hydration layer of the LNPs, causing part of the positive charge to be shielded and affecting the uptake efficiency of LNPs (Figure 8D). According to the literature, increasing the PEG percentage could promote LNP binding more molecules of water and expand their hydration layer,[26] which could change the probability of the LNPs contacting the cell membrane. Next, we evaluated the uptake efficiency and transfection ability of LNP_{G8}/pNrf2-GFP with different molecular weights of $PEGs_{(1K,\ 2K,\ and\ 5K)}$. We first determined the vesicle sizes of $LNP_{G8}(PEG_{1K})$, $LNP_{G8}(PEG_{2K})$, and $LNP_{G8}(PEG_{5K})$. The results showed that the vesicle sizes decreased with increasing PEG molecular weight (Figure 8E). As shown in Figure 8F, increasing the molecular weight of PEG increased the size of the hydration layer of the LNP preparations, making it significantly less positively charged, which was unfavorable for pDNA uptake by cells for transfection and expression. Meanwhile, the results showed that $LNP_{G8}(PEG_{1K})$ could enter cells rapidly and display GFP fluorescence in the cytoplasm compared with $LNP_{G8}(PEG_{2K})$ and $LNP_{G8}(PEG_{5K})$. These findings demonstrated that the molecular weight and percentage of PEG in the LNPs were extremely important for efficient gene transfection. Furthermore, we evaluated the uptake mechanism of $LNP_{G8}(PEG_{1K})$, $LNP_{G8}(PEG_{2K})$, and $LNP_{G8}(PEG_{5K})$, and the results indicated that they entered cells mainly by clathrin-mediated endocytosis in a time-dependent manner (Figure 8G). The transfection abilities of $LNP_{G8}(PEG_{1K})$, $LNP_{G8}(PEG_{2K})$, and $LNP_{G8}(PEG_{5K})$ were closely related to the uptake mechanism (Figure 8H). In summary, the PEG percentage changes the size of the LNP hydration layer, causing part of the positive charge to be shielded and affecting the LNP uptake efficiency. In addition, if PEG binds to too many water molecules, the chance of LNPs binding to lipid-soluble cell membranes would be reduced. Therefore, an appropriate amount of PEG in the LNPs is crucial to improve the pDNA transfection efficiency.

DISCUSSION

Gene therapy has received extensive attention recently as an effective and universal therapy for PF, but its application is severely limited by intracellular delivery efficiency. Both viral and nonviral vectors can be used to mediate gene transfection in target cells. However, the application of viral vectors carries the risks of causing host immune and inflammatory responses and carcinogenesis. Compared with viral

Figure 7. Transfection efficiency of the LNP preparations

(A) Cell viabilities of various LNPs/pDNA preparations (pDNA/LNPs = 1:5, 1:10, 1:20, and 1:50) were detected using MTT assay. (B) The uptake evaluation of DiI-labeled $LNP_{(G1–G9)}$/pECFP was investigated using CLSM. (C) The lysosome escape ability of DiI-labeled $LNP_{(G1–G9)}$/pECFP was assessed using CLSM. (D) The transfection efficiency of $LNP_{(G1–G9)}$/pECFP was evaluated using inverted fluorescence microscopy.

A

ID	$LNP_{G8}(PEG_{20\%})$	$LNP_{G8}(PEG_{10\%})$	$LNP_{G8}(PEG_{0\%})$
Particle Sizes	123.4±2.08	119.7±2.04	164.2±4.03
PDI	0.346±0.001	0.226±0.007	0.362±0.036

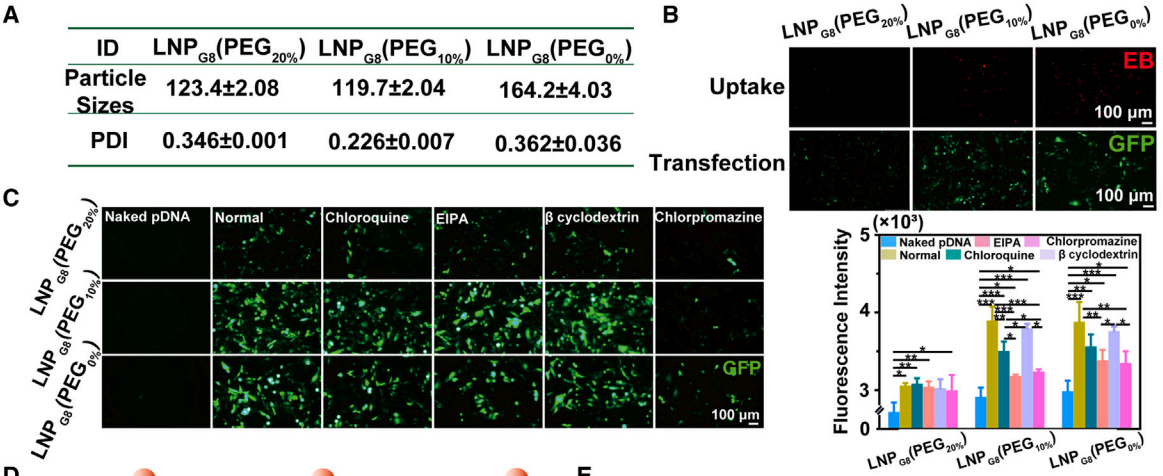

D

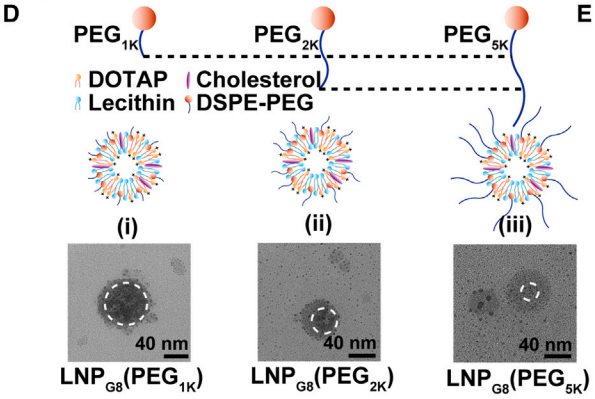

E

ID	$LNP_{G8}(PEG_{1K})$	$LNP_{G8}(PEG_{2K})$	$LNP_{G8}(PEG_{5K})$
Zeta Potential	26.93±1.01	12.97±0.26	-0.737±0.1
Particle Sizes	135.3±2.41	110.6±1.84	106.9±0.48
PDI	0.36±0.007	0.235±0.003	0.226±0.01

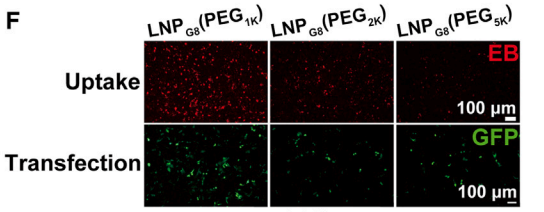

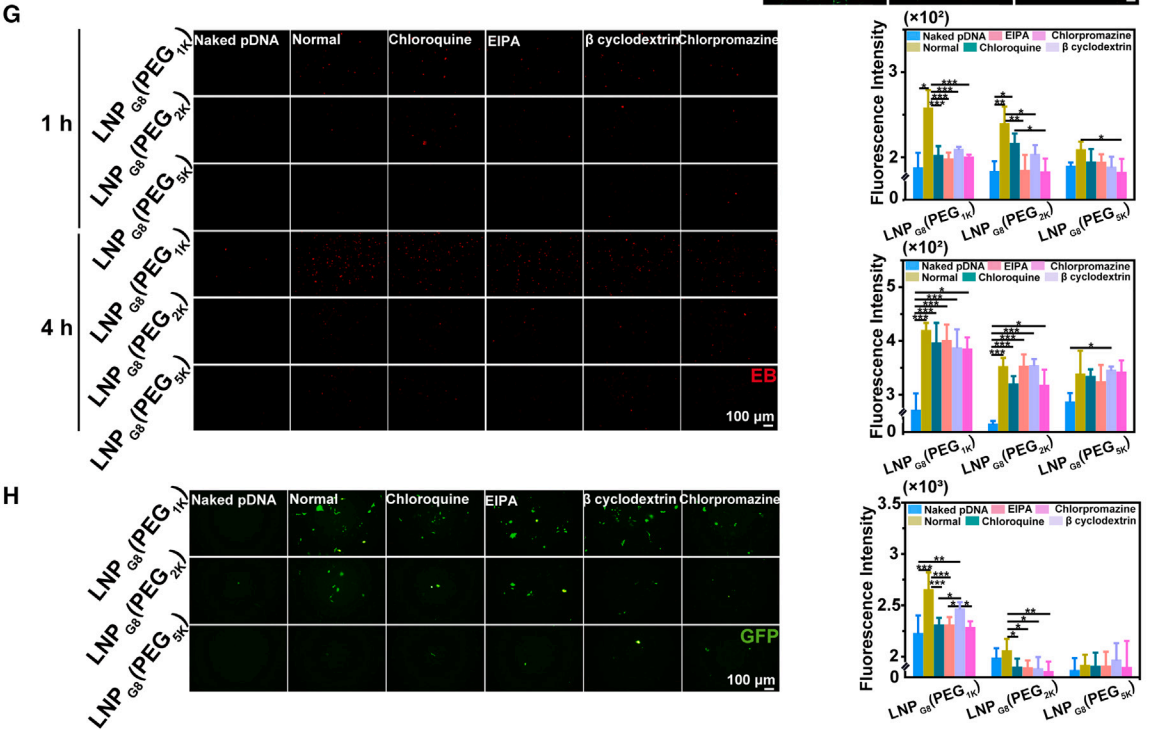

(legend on next page)

vectors, nonviral vectors are widely used in gene therapy to treat diseases because of their low immunogenicity and better genetic stability.[27] Among all nonviral vectors, the LNP platform is the best known and most widely applied,[28–30] and it is frequently used to load and deliver genes into cells. In addition to cationic lipids, which are essential excipients, cationic LNPs also include amphiphilic phospholipids, cholesterol, DSPE-PEG, and other helper phospholipids. The differences in the composition of the LNP helper phospholipids could affect the morphology, microstructure, zeta potential, and other physical and chemical properties of LNP complexes,[31–33] which may become the key factors affecting the clinical application of LNP-mediated gene transfection efficiency.

PEG has been approved by the FDA as a safe excipient, is widely used in drug delivery and has been described as an "invisible" LNP,[34] since when it is grafted on LNPs, the probability of LNPs being cleared by the MPS is reduced and the circulation time of LNPs in the blood can be improved by producing a hydration layer with a large volume. In addition, PEGylated LNPs have excellent advantages in terms of their slow aggregation in blood serum and storage stability.[35] At present, genetic drugs based on LNPs containing PEG have been developed and marketed, such as Macugen[36] and Rexin-G.[37]

Herein, we used electrostatic forces between positive and negative charges to load pDNA into LNPs for PF treatment. We systematically engineered multiple LNPs to explore the influence of different components on transfection efficiency and selected the best preparation with respect to LNP uptake behavior, lysosomal escape, and internalization capacity for antifibrosis therapy *in vitro* and *in vivo*. This study indicated that PEG could improve the accumulation of pDNA at the target sites by forming a hydration layer, which could shield the positive charge of the LNPs and prevent them from being cleared by the MPS.[38] In addition, DOTAP is a pH-sensitive cationic phospholipid that plays an important role in the cellular internalization, endosomal escape, and gene transfection efficiency of LNPs by conversion between lamellar and hexagonal conformations in aqueous solution.[39–42] However, LNPs grafted with dense PEG would bind too many water molecules and cause steric hindrance between the positive charge of DOTAP and the cell membrane, inhibiting intracellular uptake, endocytosis, and the subsequent transfection of therapeutic genes.[43,44] Therefore, to develop LNPs with high transfection efficiency *in vitro* and *in vivo*, it is necessary to not only consider the effect of the PEG molecular weight and chain length but also balance the ratio of PEG to the other carrier materials. The LNP composition is crucial parameter to allow pDNA to interact with the cell membrane and achieve endosomal escape and cytoplasmic release.[45] Our results showed that the LNP hydration layer affects gene transfection efficiency by controlling the surface charge of PEDP and influencing LNP uptake and transfection efficiency. We believe that the hydration layer that forms on highly PEGylated LNPs is the main reason why the uptake of LNPs/pDNA by cells is difficult and results in low transfection efficiency.

In this study, we first developed nine different LNPs to evaluate their *in vitro* transfection efficiency. The results demonstrated that LNP_{G8}/pECFP had the best transfection efficiency and was the most promising preparation, as it could rapidly penetrate the cell membrane barrier and significantly increase the accumulation of pECFP, showing stronger CFP fluorescence intensity than other engineered preparations (Figure 7D). Herein, we found the best transfection efficiency with the LNP_{G8} preparation, which was closely related to its composition, with the minimal PEG content being the decisive factor. This study confirmed that the percentage of PEG in LNPs could change the size of the LNP hydration layer while also shielding the positive charges, thereby reducing the delivery and transfection efficiency of the LNPs. In addition, if the molecular weight or proportion of PEG in LNPs was larger, more water molecules can bind to the LNPs, which would reduce the chance of LNP binding to the lipid-soluble cell membrane.[26,46] Therefore, it is crucial that an appropriate amount of PEG be present in the LNPs to enhance uptake and gene transfection efficiency. The behavior evaluation showed that LNP_{G8}, with the lowest PEG ratio, had the best uptake and lysosomal escape ability (Figures 7B and 7C).

To evaluate the therapeutic efficacy of PEDP, we used a disease model of PF with a complex pathological mechanism: interstitial lung disease mainly caused by abnormal accumulation of ECM in the lungs, resulting in damage to the lung structure and even death.[47] After screening the LNP preparations, we demonstrated that LNP_{G8} delivering pNrf2 and PFD (PEDP) contributed to blocking further progression of PF in model mice by alleviating oxidative stress in AECs II and inhibiting excessive collagen I accumulation. Compared with the PED (PFD-loaded) and PEP (pNrf2-loaded) groups, which could treat only injured AECs II or myofibroblasts, respectively, PEDP reversed PF through the synergistic therapeutic strategy of co-delivering genes and molecules to regulate the normalization of oxidative stress in injured AECs II and inhibit the overactivation of myofibroblasts. Importantly, adding pNrf2 to PED to generate

Figure 8. Mechanisms affecting transfection efficiency *in vitro*

(A) The vesicle sizes of $LNP_{G8}(PEG_{20\%})$, $LNP_{G8}(PEG_{10\%})$, and $LNP_{G8}(PEG_{0\%})$ were detected using the Zetasizer Nano ZS. (B) The evaluation of uptake behavior and transfection efficiency of LNP preparations were investigated using inverted fluorescence microscopy. (C) The uptake mechanism of LNP preparations was investigated using inverted fluorescence microscopy and fluorescence microplate reader. (D) The schematic of the effect of different PEGs on transfection mechanism. (E) The vesicle sizes of $LNP_{G8}(PEG_{1K})$, $LNP_{G8}(PEG_{2K})$, and $LNP_{G8}(PEG_{5K})$ were detected using the Zetasizer Nano ZS. (F) The uptake behavior and transfection efficiency of $LNP_{G8}(PEG_{1K})$/pNrf2-GFP, $LNP_{G8}(PEG_{2K})$/pNrf2-GFP, and $LNP_{G8}(PEG_{5K})$/pNrf2-GFP were investigated using inverted fluorescence microscopy. (G) Assessing the uptake mechanism of EB-stained $LNP_{G8}(PEG_{1K})$/pDNA, $LNP_{G8}(PEG_{2K})$/pDNA, and $LNP_{G8}(PEG_{5K})$/pDNA at 1 and 4 h by inverted fluorescence microscopy and fluorescence microplate reader. (H) The transfection efficiency of $LNP_{G8}(PEG_{1K})$/pNrf2-GFP, $LNP_{G8}(PEG_{2K})$/pNrf2-GFP, and $LNP_{G8}(PEG_{5K})$/pNrf2-GFP was assessed using inverted fluorescence microscopy and fluorescence microplate reader. $^{*}p < 0.05$, $^{**}p < 0.01$, and $^{***}p < 0.001$).

PEDP enhanced the therapeutic effect of PFD by reducing TGF-β expression via alleviation of AECs II oxidative stress and inhibiting the abnormal activation of intracellular inflammatory pathways. Our data showed that PEDP treatment led to high expression of pNrf2, which could effectively relieve oxidative stress in AECs II and keep cells active. This resulted in the upregulated expression of oxidative stress-related indicators, including SOD and GSH, and the downregulation of MDA expression. In addition, pNrf2 and PFD synergistically blocked PF progression by inhibiting the overproliferation of inflammatory cells and myofibroblasts in lung tissues, decreasing the accumulation of collagen I and reversing PF, which demonstrated that pNrf2 could significantly enhance the therapeutic effect of PFD. In summary, compared with the other LNPs used for transfection, PEDP showed the uniform vesicle size distribution, ideal surface charge, and well-defined nanosphere structure because of the controlled excipients composition, which could improve the accumulation of genes and molecules in fibrotic lung tissues. DOTAP is a pH-sensitive phospholipid that was inserted into PEDP that promoted the effective release of therapeutics after their rapid entry into cells and the synergistic effects of pNrf2 combined with PFD by improving gene transfection efficiency. Because of these characteristics, this system showed good biocompatibility and few side effects after tracheal administration and could protect the therapeutics from being cleared, finally leading to the reversal of PF. Additionally, using precisely controlled uncomplexed phospholipid compositions and excipients that are rarely toxic are crucial for advancing the clinical development of gene therapy for PF treatment. Herein, we propose an innovative therapeutic strategy of synergistic gene and drug delivery to regulate injured AECs II and myofibroblasts, thereby reversing PF. Therefore, this research provides a theoretical basis and practical experience for the clinical design of LNPs with efficient transfection functions.

MATERIALS AND METHODS

Materials

Lipo 3000 was purchased from Thermo Fisher Scientific. Cholesterol, lecithin, PFD, dimethyl sulfoxide (DMSO), chlorpromazine, chloroquine, β cyclodextrin, EIPA, BLM, and 2′,7′-dichlorodihydrofluorescein diacetate (DCFH-DA) were purchased from Aladdin Bio-Chem Technology (Shanghai, China). Fetal bovine serum (FBS) and RPMI 1640 were purchased from Gibco. DOTAP was purchased from A.V.T. Pharmaceutical Technology (Shanghai, China). SOD, GSH, and MDA kits were purchased from Nanjing Jiancheng Biological (Nanjing, China). α-SMA and Nrf2 kits were purchased from Shanghai Enzyme-Linked Biotechnology (Shanghai, China). DSPE-$PEG_{1,000}$, DSPE-$PEG_{2,000}$, and DSPE-$PEG_{5,000}$ were purchased from Ponsure Biotechnology (Shanghai, China). Enhance cyan fluorescent protein plasmid (pECFP-N1), pLenti-CMV-mNfe2I2-GFP-Puro (pNrf2-GFP), and pLVX-Puro-mNfe2I2 (pNrf2) were obtained from Public Protein/Plasmid Library. 4DAPI was purchased from Jiangsu KeyGEN BioTECH (Nanjing, China). Lyso-Tracker green DND 26 was purchased from Yeasen Biotechnology (Shanghai, China). EB staining solution was purchased from TIANGEN Biotech (Beijing, China). MTT was purchased from Biosharp Biotechnology (Hefei, China). Crystal violet was purchased from DAMAO Chemical Reagent Factory (Tianjin, China). E-cadherin, Nrf2 antibody, α-SMA, and β actin antibody were purchased from Servicebio (Wuhan, China). DiI was purchased from Biolite Biotechnology (Xi'an, China).

Cell lines and animals

Human lung adenocarcinoma cells (A549) and human hepatocellular carcinoma cells (SMMC 7721) were cultured in RPMI 1640 medium with 10% FBS (v/v). All the cells were incubated in a condition of 5% CO_2 at 37°C.

Male C57BL/6 mice (6–8 weeks, 20 ± 2 g) were obtained from Liaoning Changsheng Biotechnology (Benxi, China) and were carefully housed on a 12 h light and 12 h dark cycle. All of the animal experiments were performed according to the Animal Experimentation Ethics Committee of Jinzhou Medical University.

Preparation and characterization of $LNP_{(G1–G9)}$

The pDNA-loaded LNPs were prepared by emulsification-solvent evaporation followed by positive negative charge binding force method, which were composed of lecithin, cholesterol, DSPE-PEG (1,000, 2,000, or 5,000), DOTAP, and pDNA. Briefly, lecithin, cholesterol, DSPE-PEG (1,000, 2,000, or 5,000), DOTAP, and/or PFD were dissolved in anhydrous ethanol and stand at room temperature overnight to remove organic solvents. After that, nanoparticles were homogenized using ultrasonic cell disruption device for 5 min (Sonics VCX130) to obtain 9 groups of $LNP_{(G1–G9)}$. The hydrodynamic diameter, polydispersity, and zeta potential of the $LNP_{(G1–G9)}$ were measured using the Zetasizer Nano ZS. To observe the morphologies, the LNPs (20 μL) were added into a copper grid and the excess solutions were dried. The morphology changes of LNPs were photographed by transmission electron microscopy.

Preparation and of characterization $LNP_{(G1–G9)}$/pDNA complexes

Then, pDNA was added dropwise into $LNP_{(G1–G9)}$ solution to obtain pDNA-loaded LNPs through different mass ratios (1:5, 1:10, 1:20, and 1:50) of pDNA and DOTAP in the $LNP_{(G1–G9)}$. The gel electrophoresis assay was used to verify the binding rate of pDNA and LNPs. A certain amount of loading buffer was added to the prepared LNPs/pDNA complexes so that the final volume of the preparations was 20 μL. The samples were loaded on 1% agarose gel (containing 0.5 μg/mL EB solution) for 80 V, 45 min by gel electrophoresis assay. After then, the gels were imaged by the gel image system (Tanon 1600) to determine the condensation of pDNA and various LNPs.

Cytotoxicity assay *in vitro*

The A549 cells were cultured in 96-well plates with 1×10^4 cells/well overnight. The various LNPs/pDNA complexes were added into 96 wells and incubated with cells in FBS-free medium for 48 h. After that, 20 μL MTT solution (5 mg/mL) was added into medium for 4 h and the medium was aspirated, 200 μL DMSO solution was added

into the plates, and the absorbance was measured using a microplate reader. The cell viability was calculated using Equation 1:

$$\text{Cell viability}\ (\%) = \frac{A_{\text{test}} - A_{\text{blank}}}{A_{\text{control}} - A_{\text{blank}}}. \quad \text{(Equation 1)}$$

Prescription selection for optimal transfection efficiency

The various radios of LNP_{G8} and pECFP complexes were prepared to select optimal transfection efficiency. The A549 cells were cultured at 5×10^4 in 24-well plates overnight. The cells were treated with various LNP_{G8}/pECFP complexes for 4 h, and which was then replaced with a medium containing 10% FBS to incubate for 48 h. After that, the cells were observed using inverted fluorescence microscopy to evaluate the optimal transfection efficiency of various LNP_{G8}/pECFP complexes.

Uptake mechanism of DiI-labeled LNPs/pNrf2-GFP complexes

A549 cells were seeded at 1×10^4 cells/well and 5×10^4 cells/well in 96-well plates and 24-well plates overnight, respectively. First, the cells were treated with chlorpromazine (30 μM), chloroquine (30 μM), β cyclodextrin (30 μM), and EIPA (30 μM) for 1 h. The various LNP_{G8}/pNrf2-GFP complexes into 96-well plates for 4 h and then replaced with medium contain 10% FBS for 48 h. The inverted fluorescence microscopy and a microplate reader were used to observe the images and fluorescence absorbance, respectively.

Uptake rate of DiI-labeled LNPs/pDNA complexes *in vitro*

To observe the uptake rate of LNPs, A549 cells were seeded in 24-well plates at 5×10^4 cells/well overnight. The various LNP_{G8}/pDNA complexes were stained using EB solution for 30 min, and the EB-stained LNP_{G8}/pDNA was added into the plates and incubated with cells in FBS-free medium for 1 and 4 h. After that, the incubated cells were examined using CLSM and inverted fluorescence microscopy.

Lysosome escape assay

The release of genes from lysosomes to the cytoplasm is a prerequisite for promoting gene transfection and expression. A549 cells were seeded in glass bottom dishes at 5×10^4 cells/dish overnight. The prepared LNP_{G8}/pDNA complexes were stained via EB solution for 30 min, and then the stained complexes were added into the dishes and incubated with cells in FBS-free medium for 1 h, 4 h and 6 h. After that, the cells were fixed with 4% paraformaldehyde for 10 min and the lysosome of cells was stained by Lyso-Tracker green DND 26 for 1 h at 37°C. Finally, the cells were observed using CLSM.

Wounding healing assay

The A549 cells were cultured at 1×10^5 cells/well in 12-well plates overnight. After the cell density reached 80%, the scars of the same width were scraped from the cell layer with a tip of 10 μL, and washed with PBS to remove the adherent cells. First, the cells were treated with H_2O_2 (500 μM) for 12 h, then PED, PEP, and PEDP (pNrf2 = 10 μg/well) were added into various plates and incubated with cells for 48 h. The therapeutic efficacy was detected via inverted fluorescence microscopy.

Transwell migration assay

The Transwell migration assay was carried out to evaluate the migration ability of oxidative stress cells. A549 cells were seeded in the upper chamber of 8 μm pore size and cultured with 600 μL of RPMI 1640 medium containing 10% FBS, and lower chamber was 800 μL of RPMI 1640 medium with free FBS. Initially, the cells were treated with H_2O_2 (500 μM) for 12 h and incubated with PED, PEP, and PEDP (pNrf2 = 10 μg/well) for 48 h. And next, the cells were stained with 0.1% crystal violet for 30 min and gently wipe off the cells in the upper chamber layer. Finally, outer cells of the upper chamber were observed via inverted fluorescence microscopy.

Immunofluorescence staining *in vitro*

The A549 cells were seeded in 6-well plates containing sterile round coverslip at 2×10^5 cells/well overnight. Before treating, the cells were incubated with H_2O_2 (500 μM) for 12 h, then PED, PEP, and PEDP (pNrf2 = 10 μg/well) were added into different wells and treated with cells for 48 h. After that, the cells were fixed 4% paraformaldehyde for 10 min, immunofluorescence staining was then used to evaluate protein expression of Nrf2 and E-cadherin.

Determination of intracellular ROS content *in vitro*

Excessive oxidative stress is an important factor in the transformation of alveolar epithelial cells into mesenchymal stem cells (EMT). DCFH-DA was performed to evaluate the expression of ROS. The A549 cells were seeded into 24-well plates at 5×10^4 cells/well overnight. The cells were pretreated with H_2O_2 (500 μM) for 12 h, and then the cells were incubated with various groups of PED, PEP, and PEDP (pNrf2 = 10 μg/well) for 48 h. Next, DCFH-DA (5 μM) was added into the plates to incubate with cells for 0.5 h, and the fluorescence of the plates was evaluated using inverted fluorescence microscopy.

Determination of intracellular MMP content *in vitro*

The A549 cells were seeded at 5×10^4 cells/well in glass bottom dishes. The cells were pretreated with H_2O_2 (500 μM) for 12 h, and then the cells were incubated with various groups of PED, PEP, and PEDP (pNrf2 = 10 μg/well) for 48 h. Next, the JC-1 reagent was added into the plates to incubate with cells for 0.5 h. After that, the treated cells were fixed with 4% paraformaldehyde for 10 min and evaluated using CLSM to observe the therapeutic efficacy.

Construction of PF mice model

Mice were reared adaptively for one week before modeling. After that, C57BL/6 mice were first anesthetized with 10% chloral hydrate (70 μL), and bleomycin sulfate (5 mg/kg) was then perfused into the mice trachea by tracheal delivery device.

Biodistribution assay *in vivo*

In vivo imaging of mice was performed to evaluate the biodistribution of LNP_{G8}/pDNA complexes in normal mice and fibrotic mice, and DiI was as a model fluorescent drug for LNP_{G8}/pDNA complexes tracking. The DiI-labeled LNP_{G8}/pNrf2 complexes were administrated into the mice after developing PF by tracheal administration.

The distribution of DiI-labeled LNP_{G8}/pNrf2 in two groups of mice was observed using IVIS Spectrum at different times (1, 8, and 24 h). After that, the mice were sacrificed and major organs were removed to detect and the fluorescence intensity.

In addition, the immunofluorescence staining was used to evaluate the target ability of LNP_{G8}/pNrf2-GFP to AECs II. First, LNP_{G8}/pNrf2-GFP were injected into the mice by tracheal administration. After 48 h later, the mice were sacrificed and fixed with 4% paraformaldehyde overnight. The AECs II in the lungs were labeled with SPC with 1:500 by immunofluorescence staining, and the operations process referred to immunofluorescence staining assay.

Antifibrosis efficacy *in vivo*

The PF mice were divided into 5 groups (n = 5) and administrated with various preparations through tracheal administration once every two days for a total of 4 times with concomitant monitoring, and treatment would last for 3 weeks. The dosages of the different formulations are as follows: (1) PF, (2) normal, (3) PED (PFD = 10 mg/kg), (4) PEP (pNrf2 = 20 μg/mouse), and (5) PEDP (pNrf2 = 20 μg/mouse and PFD = 10 mg/kg). The body weight of mice was measured every day to evaluate the therapeutic effect. After the treatment, the mice were anesthesia and the peripheral blood was removed from the orbit of the mice, then mice were euthanized. One of the lungs was fixed with 4% paraformaldehyde for immunofluorescent staining detection, and the others were frozen in liquid nitrogen for the detection of biochemical index. The fixed lungs, hearts, spleens, livers, and kidneys in different groups were stained by H&E staining and Masson trichrome staining, and the expressions of Nrf2, E-cadherin, collagen I, and α-SMA were detected by immunofluorescent staining. AST, ALT, and BUN were examined by automatic biochemical analyzer to assess the biosafety of the preparations.

Statistical analysis

All experiments were performed at least three times. The differences among multiple groups were determined using one-way ANOVA in SPSS 22.0; two independent groups were analyzed using Student's t test. p values >0.05 indicated no significance (N.S.), and p values < 0.05 indicated statistical significance between two groups.

DATA AVAILABILITY

The data that support the findings of this study are available from the corresponding author (X.C.) upon reasonable request.

SUPPLEMENTAL INFORMATION

Supplemental information can be found online at https://doi.org/10.1016/j.omtn.2023.04.006.

ACKNOWLEDGMENTS

We thank the support of Liaoning Provincial Key Laboratory of Marine Bioactive Substances and Technological Innovation Center of Liaoning Pharmaceutical Action and Quality Evaluation. This work was funded by the National Natural Science Foundation of China (grant 82104111), the Youth Project of Liaoning Provincial Department of Education (grant LJKQZ2021146), and the Foundation of Department of Education of Liaoning Province (grant JYTJCZR2020069).

AUTHOR CONTRIBUTIONS

X.C. and H.-L.J. designed and supervised the experiments. X.C., B.G., and H.-L.J. wrote the manuscript. X.C., Y.-M.H., and Q.-L.L. performed the experiments. X.C. and C.L. analyzed the data. All authors contributed to interpret the results.

DECLARATION OF INTERESTS

All the authors declare no competing interests.

REFERENCES

1. Somogyi, V., Chaudhuri, N., Torrisi, S.E., Kahn, N., Muller, V., and Kreuter, M. (2018). The therapy of idiopathic pulmonary fibrosis: what is next? Eur. Respir. Rev. *28*, 190021.

2. Ji, Q.J., Hou, J.W., Yong, X.Q., Gong, M., Muddassir, M., Tang, T.Y., Xie, J.B., Fan, W.P., and Chen, X.Y. (2021). Targeted dual small interfering ribonucleic acid delivery via non-viral polymeric vectors for pulmonary fibrosis therapy. Adv. Mater. *33*, e2007798.

3. Lederer, D.J., Martinez, F.J., Harold, R.C., Annie, P., Ganesh, R., Luca, R., Moises, S., Jeffrey, J.S., Hiroyuki, T., and Athol, U.W. (2018). Idiopathic pulmonary fibrosis. Nat. Rev. Dis. Primers *378*, 1811–1823.

4. D'alessandro-Gabazza, C.N., Yasuma, T., Kobayashi, T., Toda, M., Abdel-Hamid, A.M., Fujimoto, H., Hataji, O., Nakahara, H., Takeshita, A., Nishihama, K., et al. (2022). Inhibition of lung microbiota-derived proapoptotic peptides ameliorates acute exacerbation of pulmonary fibrosis. Nat. Commun. *13*, 1558.

5. Hecker, L., Logsdon, N.J., Kurundkar, D., Kurundkar, A., Bernard, K., Hock, T., Meldrum, E., Sanders, Y.Y., and Thannickal, V.J. (2014). Reversal of persistent fibrosis in aging by targeting NOX4-Nrf2 redox imbalance. Sci. Transl. Med. *6*, 231ra47.

6. Ogger, P.P., Albers, G.J., Hewitt, R.J., O'Sullivan, B.J., Powell, J.E., Calamita, E., Ghai, P., Walker, S.A., McErlean, P., Saunders, P., et al. (2020). Itaconate controls the severity of pulmonary fibrosis. Sci. Immunol. *5*, eabc1884.

7. Kaner, R.J., Bajwa, E.K., El-Amine, M., Gorina, E., Gupta, R., Lazarus, H.M., Luckhardt, T.R., Mouded, M., Posada, K., Richeldi, L., et al. (2019). Design of idiopathic pulmonary fibrosis clinical trials in the era of approved therapies. Am. J. Respir. Crit. Care Med. *200*, 133–139.

8. Pitre, T., Mah, J., Helmeczi, W., Khalid, M.F., Cui, S., Zhang, M., Husnudinov, R., Su, J., Banfield, L., Guy, B., et al. (2022). Medical treatments for idiopathic pulmonary fibrosis: a systematic review and network meta-analysis. Thorax *77*, 1243–1250.

9. Paôline, L., Allard, B., Manicki, P., Valérie, J., Levionnois, E., Jeljeli, M., Henrot, P., Izotte, J., Leleu, D., Groppi, A., et al. (2021). TGF-β promotes low IL10-producing ILC2 with profibrotic ability involved in skin fibrosis in systemic sclerosis. Ann. Rheum. Dis. *80*, 1594–1603.

10. Wang, G., Chen, S., Qiu, N., Wu, B., Zhu, D., Zhou, Z., Piao, Y., Tang, J., and Shen, Y. (2021). Virus-mimetic DNA-ejecting polyplexes for efficient intracellular cancer gene delivery. Nano Today *39*, 101215.

11. Dane, E.L., Belessiotis-Richards, A., Backlund, C., Wang, J., Hidaka, K., Milling, L.E., Bhagchandani, S., Melo, M.B., Wu, S., Li, N., et al. (2022). STING agonist delivery by tumour-penetrating PEG-lipid nanodiscs primes robust anticancer immunity. Nat. Mater. *21*, 710–720.

12. Moncal, K.K., Tigli Aydın, R.S., Godzik, K.P., Acri, T.M., Heo, D.N., Rizk, E., Wee, H., Lewis, G.S., Salem, A.K., and Ozbolat, I.T. (2022). Controlled co-delivery of pPDGF-B and pBMP-2 from intraoperatively bioprinted bone constructs improves the repair of calvarial defects in rats. Biomaterials *281*, 121333.

13. Wittrup, A., and Lieberman, J. (2015). Knocking down disease: a progress report on siRNA therapeutics. Nat. Rev. Genet. *16*, 543–552.

14. Jiang, C., Chen, J., Li, Z., Wang, Z., Zhang, W., and Liu, J. (2019). Recent advances in the development of polyethylenimine-based gene vectors for safe and efficient gene delivery. Expert Opin. Drug Deliv. *16*, 363–376.

15. Mohammadinejad, R., Dehshahri, A., Sagar Madamsetty, V., Zahmatkeshan, M., Tavakol, S., Makvandi, P., Khorsandi, D., Pardakhty, A., Ashrafizadeh, M., Ghasemipour-Afshar, E., et al. (2020). *In vivo* gene delivery mediated by non-viral vectors for cancer therapy. J. Control. Release *325*, 249–275.

16. Sizovs, A., Xue, L., Tolstyka, Z.P., Ingle, N.P., Wu, Y., Cortez, M., and Reineke, T.M. (2013). Poly(trehalose): sugar-coated nanocomplexes promote stabilization and effective polyplex-mediated siRNA delivery. J. Am. Chem. Soc. *135*, 15417–15424.

17. Wang, C., Liu, Q., Zhang, Z., Wang, Y., Zheng, Y., Hao, J., Zhao, X., Liu, Y., and Shi, L. (2021). Tumor targeted delivery of siRNA by a nano-scale quaternary polyplex for cancer treatment. Chem. Eng. J. *425*, 130590.

18. Sun, C.Y., Shen, S., Xu, C.F., Li, H.J., Liu, Y., Cao, Z.T., Yang, X.Z., Xia, J.X., and Wang, J. (2015). Tumor acidity-sensitive polymeric vector for active targeted siRNA delivery. J. Am. Chem. Soc. *137*, 15217–15224.

19. Javadi, A., Jamil, T., Abouzari-Lotf, E., Soucek, M.D., and Heinz, H. (2021). Working mechanisms and design principles of comb-like polycarboxylate ether superplasticizers in cement hydration: quantitative insights for a series of well-defined copolymers. ACS Sustain. Chem. Eng. *9*, 8354–8371.

20. Wang, Y., Guo, R., Wang, H., Liang, B., Du, Y., Lau, W.B., Gao, E., Christopher, T., Lopez, B., and Ma, X.L. (2017). Adiponectin regulates microRNA449b/NFE2L1 endogenous antioxidative pathway, to ameliorate cardiac ischemia reperfusion injury in diabetic mice. Circulation *136*, 222–233.

21. Mashima, K., Sato, K., Takayama, N., Izawa, J., Ikeda, T., Umino, K., Nakano, H., Minakata, D., Morita, K., Yamamoto, C., et al. (2020). Dimethyl fumarate ameliorates graft-versus-host disease by negatively regulating aerobic glycolysis in alloreactive T-cells. Blood *136*, 24–25.

22. Tanner, L., Single, A.B., Bhongir, R.K.V., Heusel, M., Mohanty, T., Karlsson, C.A.Q., Pan, L., Clausson, C.M., Bergwik, J., Wang, K., et al. (2023). Small-molecule-mediated OGG1 inhibition attenuates pulmonary inflammation and lung fibrosis. Nat. Commun. *14*, 643.

23. Burman, A., Tanjore, H., and Blackwell, T.S. (2018). Endoplasmic reticulum stress in pulmonary fibrosis. Matrix Biol. *68-69*, 355–365.

24. Chang, X., Xing, L., Wang, Y., Yang, C.X., He, Y.J., Zhou, T.J., Gao, X.D., Li, L., Hao, H.P., and Jiang, H.L. (2020). Monocyte-derived multipotent cell delivered programmed therapeutics to reverse idiopathic pulmonary fibrosis. Sci. Adv. *6*, eaba3167.

25. Liu, Z., Wang, S., Tapeinos, C., Torrieri, G., Känkänen, V., El-Sayed, N., Python, A., Hirvonen, J.T., and Santos, H.A. (2021). Non-viral nanoparticles for RNA interference: principles of design and practical guidelines. Adv. Drug Deliv. Rev. *174*, 576–612.

26. Tirosh, O., Barenholz, Y., Katzhendler, J., and Priev, A. (1998). Hydration of polyethylene glycol-grafted liposomes. Biophys. J. *74*, 1371–1379.

27. Qi, L.Y., Wang, Y., Hu, L.F., Zhao, P.S., Yu, H.Y., Xing, L., Gao, X.D., Cao, Q.R., and Jiang, H.L. (2022). Enhanced nuclear gene delivery via integrating and streamlining intracellular pathway. J. Control. Release *341*, 511–523.

28. Chang, X., Xing, L., Wang, Y., Zhou, T.J., Shen, L.J., and Jiang, H.L. (2020). Nanoengineered immunosuppressive therapeutics modulating M1/M2 macrophages into the balanced status for enhanced idiopathic pulmonary fibrosis therapy. Nanoscale *12*, 8664–8678.

29. Robinson, E., MacDonald, K.D., Slaughter, K., McKinney, M., Patel, S., Sun, C., and Sahay, G. (2018). Lipid nanoparticle-delivered chemically modified mRNA restores chloride secretion in cystic fibrosis. Mol. Ther. *26*, 2034–2046.

30. Basha, G., Cottle, A.G., Pretheeban, T., Chan, K.Y., Witzigmann, D., Young, R.N., Rossi, F.M., and Cullis, P.R. (2022). Lipid nanoparticle mediated silencing of osteogenic suppressor GNAS leads to osteogenic differentiation of mesenchymal stem cells *in vivo*. Mol. Ther. *30*, 3034–3051.

31. Garenne, D., Libchaber, A., and Noireaux, V. (2020). Membrane molecular crowding enhances MreB polymerization to shape synthetic cells from spheres to rods. Proc. Natl. Acad. Sci. USA *117*, 1902–1909.

32. Zhao, Y., Liu, A., Du, Y., Cao, Y., Zhang, E., Zhou, Q., Hai, H., Zhen, Y., and Zhang, S. (2018). Effects of sucrose ester structures on liposome-mediated gene delivery. Acta Biomater. *72*, 278–286.

33. Yuba, E., Kojima, C., Sakaguchi, N., Harada, A., Koiwai, K., and Kono, K. (2008). Gene delivery to dendritic cells mediated by complexes of lipoplexes and pH-sensitive fusogenic polymer-modified liposomes. J. Control. Release *130*, 77–83.

34. Suk, J.S., Xu, Q., Kim, N., Hanes, J., and Ensign, L.M. (2016). PEGylation as a strategy for improving nanoparticle-based drug and gene delivery. Adv. Drug Deliv. Rev. *99*, 28–51.

35. Stavnsbjerg, C., Christensen, E., Münter, R., Henriksen, J.R., Fach, M., Parhamifar, L., Christensen, C., Kjaer, A., Hansen, A.E., and Andresen, T.L. (2022). Accelerated blood clearance and hypersensitivity by PEGylated liposomes containing TLR agonists. J. Control. Release *342*, 337–344.

36. Shigdar, S., Schrand, B., Giangrande, P.H., and de Franciscis, V. (2021). Aptamers: cutting edge of cancer therapies. Mol. Ther. *29*, 2396–2411.

37. Chawla, S.P., Bruckner, H., Morse, M.A., Assudani, N., Hall, F.L., and Gordon, E.M. (2019). A phase I-II study using rexin-G tumor-targeted retrovector encoding a dominant-negative cyclin G1 inhibitor for advanced pancreatic cancer. Mol. Ther. Oncolytics *12*, 56–67.

38. McSweeney, M.D., Wessler, T., Price, L.S.L., Ciociola, E.C., Herity, L.B., Piscitelli, J.A., Zamboni, W.C., Forest, M.G., Cao, Y., and Lai, S.K. (2018). A minimal physiologically based pharmacokinetic model that predicts anti-PEG IgG-mediated clearance of PEGylated drugs in human and mouse. J. Control. Release *284*, 171–178.

39. Smisterová, J., Wagenaar, A., Stuart, M.C., Polushkin, E., ten Brinke, G., Hulst, R., Engberts, J.B., and Hoekstra, D. (2001). Molecular shape of the cationic lipid controls the structure of cationic lipid/dioleylphosphatidylethanolamine-DNA complexes and the efficiency of gene delivery. J. Biol. Chem. *276*, 47615–47622.

40. Nosova, A.S., Koloskova, O.O., Nikonova, A.A., Simonova, V.A., Smirnov, V.V., Kudlay, D., and Khaitov, M.R. (2019). Diversity of PEGylation methods of liposomes and their influence on RNA delivery. Medchemcomm *10*, 369–377.

41. Rädler, J.O., Koltover, I., Salditt, T., and Safinya, C.R. (1997). Structure of DNA-cationic liposome complexes: DNA intercalation in multilamellar membranes in distinct interhelical packing regimes. Science *275*, 810–814.

42. Dan, N., and Danino, D. (2014). Structure and kinetics of lipid-nucleic acid complexes. Adv. Colloid Interface Sci. *205*, 230–239.

43. Dong, R., Liu, R., Gaffney, P.R.J., Schaepertoens, M., Marchetti, P., Williams, C.M., Chen, R., and Livingston, A.G. (2019). Sequence-defined multifunctional polyethers via liquid-phase synthesis with molecular sieving. Nat. Chem. *11*, 136–145.

44. Eş, I., Montebugnoli, L.J., Filippi, M.F.P., Malfatti-Gasperini, A.A., Radaic, A., de Jesus, M.B., and de la Torre, L.G. (2020). High-throughput conventional and stealth cationic liposome synthesis using a chaotic advection-based microfluidic device combined with a centrifugal vacuum concentrator. Chem. Eng. J. *382*, 122821.

45. Berger, M., Lechanteur, A., Evrard, B., and Piel, G. (2021). Innovative lipoplexes formulations with enhanced siRNA efficacy for cancer treatment: where are we now? Int. J. Pharm. *605*, 120851.

46. Venkataraman, S., Ong, W.L., Ong, Z.Y., Joachim Loo, S.C., Ee, P.L.R., and Yang, Y.Y. (2011). The role of PEG architecture and molecular weight in the gene transfection performance of PEGylated poly(dimethylaminoethyl methacrylate) based cationic polymers. Biomaterials *32*, 2369–2378.

47. Yang, M.Y., Lin, Y.J., Han, M.M., Bi, Y.Y., He, X.Y., Xing, L., Jeong, J.H., Zhou, T.J., and Jiang, H.L. (2022). Pathological collagen targeting and penetrating liposomes for idiopathic pulmonary fibrosis therapy. J. Control. Release *351*, 623–637.